

Production of hydroxyapatite–bacterial cellulose nanocomposites from agroindustrial wastes

Eden B. Duarte · Bruna S. das Chagas · Fábíia K. Andrade · Ana I. S. Brígida · Maria F. Borges · Celli R. Muniz · Men de Sá M. Souza Filho · João P. S. Morais · Judith P. A. Feitosa · Morsyleide F. Rosa

Received: 22 March 2015 / Accepted: 14 August 2015 / Published online: 21 August 2015
© Springer Science+Business Media Dordrecht 2015

Abstract In the present work, bionanocomposites based on bacterial cellulose (BC) obtained from alternative sources (cashew juice and sisal liquid waste) and hydroxyapatite (HA) were developed. BC–HA composites were prepared through alternate immersion in CaCl_2 and Na_2HPO_4 solutions. Cellulose was successfully produced from the alternative sources of media without the need for additional supplementation and HA crystals that homogeneously precipitated onto the BC surface. The Ca/P ratio ranged from 1.53 to 1.58, indicating the presence of calcium-deficient HA in the composites; this is a phase similar to biological apatite. After

immersion into synthetic body fluid, the HA layer formed on the surface of pure BC and the composites, attesting the material's bioactivity. Moreover, apatite deposition on the composites was up to three times higher than observed on pure cellulose with no significant desorption of apatite from the composites. These results support that the BC derived from agroindustrial wastes have potential to produce nanocomposites of cellulose/HA for use in bone tissue regeneration.

Keywords *Agave sisalana* · *Anacardium occidentale* · In vitro test · Agribusiness · Nanotechnology

E. B. Duarte · B. S. das Chagas · J. P. A. Feitosa
Federal University of Ceará, Campus do Pici, Fortaleza,
CE 60455-760, Brazil

F. K. Andrade · M. F. Borges · C. R. Muniz ·
M. de Sá M. Souza Filho · M. F. Rosa (✉)
Embrapa Tropical Agroindustry, Rua Dra. Sara Mesquita,
2270, Planalto do Pici, Fortaleza, CE 60511-110, Brazil
e-mail: morsyleide.rosa@embrapa.br

A. I. S. Brígida
Embrapa Food Technology, Av. das Américas, 29.501,
Guaratiba, Rio de Janeiro, RJ 23020-470, Brazil

J. P. S. Morais
Embrapa Cotton, Rua Oswaldo Cruz, 1.143, Centenário,
Campina Grande, PB 58428-095, Brazil

Introduction

Annually, millions of people suffer from bone defects caused by trauma, tumors, or bone related diseases. Auto- and allografts bones have traditionally been the main sources for bone substitutes, in which autografts have the most osteogenic potential followed by allografts. However, the former is limited by donor-site morbidity and supply, whereas the latter may carry the risk of disease transmission and immune response (Moore et al. 2001). These concerns have led to the search for alternatives through the development of synthetic grafts.

The ideal bone graft must meet a number of requirements. They must provide enough mechanical

support without being overly stiff, be capable of integrating with the host bony tissue, be biocompatible, enhance bone regeneration, and improve the biomechanical stability of the treated bony defects (Giannoudis et al. 2005; Janicki and Schmidmaier 2011). Hydroxyapatite (HA) is widely used as a biomaterial in various biomedical applications due to their biocompatibility and osteoinductive properties; several studies revealed that nanocomposites of cellulose/HA exhibit many of these required properties, and are thus promising for applications in bone regeneration (Fang et al. 2009; Fricain et al. 2002; Grande et al. 2009; He et al. 2012; Nge et al. 2010; Saska et al. 2011; Zadegan et al. 2011; Zimmermann et al. 2011).

Bacterial cellulose (BC) produced by *Acetobacter* organisms is a biomaterial that has garnered interest in the field of tissue engineering due to its unique properties, including high water holding capacity, crystallinity, purity, and tensile strength. The in vivo biocompatibility of BC was also evaluated (Andrade et al. 2012; Helenius et al. 2006; Pértile et al. 2012; Schumann et al. 2009; Wippermann et al. 2009). Although chemically identical to plant cellulose, BC has a unique ultrafine fibrillar nanostructure, which determines its superior physical and mechanical properties. Moreover, BC is also distinguished amongst plant-derived celluloses in that it is environmentally safer. Plant-derived cellulose usually requires the removal of hemicellulose and lignin, which cause environmental damage from the use of environmentally harsh purifying techniques like Kraft pulping (Andrade et al. 2010). BC is usually produced using synthetic culture media that contains glucose as a main carbon source and other nutrients; these results in high production costs, limiting the use of this material (Gomes et al. 2013; Wu and Liu 2013). Culture medium may represent about 30 % of the total cost of microbial fermentation processes (Rivas et al. 2004).

Therefore, the use of cheaper nutrient sources, such as agroindustrial residues, is a strategy to overcome this limitation (Gomes et al. 2013; Cavka et al. 2013), favoring large-scale, low cost production and reducing the environmental impact (Huang et al. 2014). Therefore, the aim of this work was the development of a bionanocomposite based on HA and BC from alternative sources, including cashew juice and sisal juice (sisal liquid waste).

Experimental section

Microorganism and bacterial cellulose production from agroindustrial wastes

Gluconacetobacter hansenii (CCT 1431) purchased from Coleção de Culturas Tropical da Fundação André Tosello (Campinas-SP, Brazil) was used as the BC producing bacteria. Sisal and cashew juices were provided by Embrapa Algodão (Campina Grande-PB, Brazil) and Embrapa Agroindústria Tropical (Pacajus-CE, Brazil), respectively. The agroindustrial materials were filtered through a commercial fabric filter to remove debris and autoclaved (121 °C, 15 min). The pH and °Brix values from the juices were determined before bacterial cultivation. The synthetic medium (Hestrin and Schramm 1954) was used as reference medium.

The inoculum was cultivated in HS medium at 30 °C for 48 h. The reference and alternative media were cultured with 3 % (v/v) of the inoculum and statically incubated at 30 °C for 7 days. After fermentation, BC pellicles were purified through immersion in 2 % (w/v) SDS (200 mL, 25 °C, 1 min), then washed with water, followed by 4 % (w/v) NaOH treatment (600 mL, at 80 °C, 30 min). After purification, the BC pellicles were washed several times with distilled water until neutral pH was achieved.

Preparation of bacterial cellulose/hydroxyapatite nanocomposites

The BC–HA composites were prepared according to Hutchens et al. (2006). After purification, the BC pellicles (21 × 13 cm), with thickness of about 15 µm, were immersed in 800 mL of CaCl₂ solution (11 g L⁻¹) and mildly stirred at 30 °C for 24 h. Thereafter, for the removal of excess CaCl₂, the pellicles were washed with deionized water, followed by immersion in 800 mL of Na₂HPO₄ solution (8.52 g L⁻¹) using the same conditions previously described. This alternate soaking process (immersion in calcium and phosphate solutions) was repeated six times with the samples rinsed thoroughly with deionized water between each soaking cycle (~500 mL of deionized water for 10 min at 25 °C). Finally, these nanocomposites were removed, dried in an air oven at 70 °C to a constant weight and stored in a desiccator until use.

The nanocomposites obtained from the BC pellicles produced in HS, sisal liquid, and cashew juice were designated as HS-HA, Sisal-HA and Cashew-HA, respectively.

Thermal analyses (TGA/dTG)

Thermal analyses (TGA and dTG) were performed on a thermogravimetric analyzer (Shimadzu, TGA STA 6000), with 5–7 mg of dried samples in the range of 0–700 °C under a nitrogen atmosphere (40 mL/min) at a heating rate of a 10 °C min⁻¹ to evaluate their thermal stability.

X-ray diffraction

X-ray diffraction analyses were performed on an X-ray diffractometer (Rigaku, DMAXB), using CuK α radiation. The diffraction data were collected in the 2 θ range from 10° to 40° at a scanning speed of 0.5° min⁻¹. The crystallinity index (CI) is a measure of the percentage of crystalline material in a given sample and it is also correlated to the degree of order within the crystals. Cellulose crystallinity index was determined as described by Segal et al. (1959), and the HA crystalline index was calculated using the Landi et al. (2000) method (Segal et al. 1959; Landi et al. 2000). The crystalline species (cellulose and HA) were identified using the X-pert Highscore 1.0 and comparison of the XRD pattern of each sample on the database (JCPDS).

Fourier transform infrared spectroscopy (FTIR) studies

Samples were examined using a Fourier transform infrared spectrometer (FTIR, Nicolet 800 combined with a MTEch PAS cell). Samples were ground and pelletized using KBr (1:10, w/wt), followed by uniaxillary pressure under vacuum. Spectra were obtained between 4000 and 400 cm⁻¹ at a 4 cm⁻¹ of resolution.

SEM and EDS

Cellulose pellicles and CB-HA composites were analyzed by scanning electron microscopy (SEM) on a Zeiss DSM-940^A microscope at 30 kV after gold-sputtering treatment. The average diameters of the

nanofibers and globular crystals of at least 50 structures were determined using the ImageJ program (National Institute of Health-NIH). Energy dispersive X-ray spectroscopy (EDS) was used to determine the C/O molar ratio from purified BC pellicles and the Ca/P molar ratio from the composites.

Desorption study

Desorption was assessed by measuring the variation of weight loss, attributed to apatite release, from the composite. Samples that were 1 cm² in size, were weighed and immersed in 0.1 mol L⁻¹ phosphate buffered solution (PBS) at pH 7.25 and 37 °C for 30 days. After, the samples were washed with deionized water, dried in an air oven at 70 °C to a constant weight.

Bioactivity assessment

A bioactivity assay was developed using the synthetic body fluid (SBF) technique described by Bohner and Lemaître (2009). Nanocomposite samples (4 cm²) were completely immersed in 40 mL of SBF at 37 °C for 14 days. The samples were then dried in an air oven at 70 °C to a constant weight. The amount of deposited apatite on the composite surface was determined by the mass difference between the initial and the final mass.

Protein (BSA) adsorption

BSA Adsorption onto the composite materials was performed as described by Bundela and Bharadwaj (2012). Fresh BSA solutions (0.5 mg mL⁻¹) were prepared in 0.5 M PBS (Phosphate Buffer Solution) at pH 7.4. The composite samples (200 mg) were equilibrated with PBS for 24 h and then gently shaken for 120 min. The composites were removed, and the concentration of non-adsorbed protein in the liquid medium was measured by recording the absorbance of protein solution at 272 nm with a UV spectrophotometer (Cirrus 60 ST, Femto) and quantified using a BSA standard curve.

Statistical analysis

The statistical analysis was carried out using the software OriginPro 7.0 (OriginLab Corporation). Each

assay was conducted in triplicate. The statistical significance of the evaluated data was analyzed by one-way analysis of variance (ANOVA) and an unpaired *F*-test. The values were considered significant when $\alpha < 0.05$.

Results and discussion

Bacterial cellulose production from agroindustrial wastes

The agroindustrial wastes had a combination of °Brix and pH close to the HS medium (Table 1).

In the °Brix analysis for sugar content estimation, the nearly equivalent values between the alternative media and the standard medium suggest the existence of carbohydrates in the cashew and sisal juices that can be used by *G. hansenii* for the metabolic process. Both juices maintained a pH close to 5, which was within the optimum pH range (4–6) for *Gluconacetobacter* growth (Chawla et al. 2009). After the production and purification, all the pellicles were gelatinous, resistant to handling, and translucence. The yield of BC production from HS and sisal juice was about the same (0.54 g L⁻¹) as well as their microfibrillar network structure. BC obtained from cashew juice presented the minor yield (~0.28 g L⁻¹) with loosely network structure.

Thermal analyses (TGA/dTG)

The first instance of mass loss for the BC pellicles (4–6 %) and for the BC–HA composites (6–11 %) occurred around 100 °C due to the evaporation of water adsorbed on the cellulose. Between 280 and 310 °C (Table 2), there was another mass loss event caused by the cellulose degradation processes (depolymerization, dehydration, and decomposition of the glycoside units) followed by carbonic residue formation (Saska et al. 2011; Barud et al. 2007, 2008a;

Table 1 °Brix and pH values determined for the culture media

Medium	°Brix	pH
HS	10.8 ± 0.03	5.05 ± 0.02
Cashew	10.1 ± 0.01	4.42 ± 0.04
Sisal	12.0 ± 0.02	4.82 ± 0.02

Table 2 Percentage of mass loss of BC and BC–HA composites for the cellulose degradation thermal event

	HS	Cashew juice	Sisal juice
<i>Bacterial cellulose</i>			
T _{onset} (°C)	304	294	299
T _{peak} (°C)	340	341	332
Residue at 700 °C (%)	25.7	22.6	26.0
<i>Bacterial cellulose–hydroxyapatite composite</i>			
T _{onset} (°C)	302	305	305
T _{peak} (°C)	331	339	340
Residue at 700 °C (%)	72.5	67.8	66.0

Wan et al. 2007) Although this thermal event is the main characteristic of cellulose degradation, these mass losses are not fixed values, and they depend on the cellulosic source (Uesu et al. 2000). In general, the HA has thermal stability in this temperature range. The decomposition of HA is usually accompanied by a phase change, and tends to be evidenced at temperatures above 700 °C, which leads to a high amount of residues. After the analysis, a carbonaceous residue around 24.8 % was observed for BC samples, whereas the BC–HA composites exhibited a residue around 68.1 %. This evidence confirms HA deposition on the BC membrane, and the HA content was estimated to be around 43.3 %. Table 2 presents the percentages of the 2nd mass loss (2nd event) and their respective temperatures for pure BC and BC–HA composites (Fig. 1).

X-ray diffraction

The BC (Fig. 2) displayed three diffraction peaks at $2\theta = 15^\circ$, 17° , and 22.5° , which are usually attributed to the interplanar distance characteristic of I α and I β phases of elementary crystalline structure of cellulose. Planes (100)_{I α} , (110)_{I β} , and (010)_{I β} are related to the angle of 15° , whereas the planes (110)_{I α} and (200)_{I β} are associated to the angle 22.5° (Saska et al. 2011; Barud et al. 2008b). The absence of a high-intensity peak at 34.5° indicates that the sample is mainly composed of I α cellulose. The CI of the BC pellicles were 77.4 % for HS, 69.3 % for cashew, and 72.7 % for sisal. These values are within the expected crystallinity range (Andrade et al. 2010).

In the BC–HA composites, there were peaks at $2\theta = 15^\circ$ and 22.5° , as similar to the neat pellicles

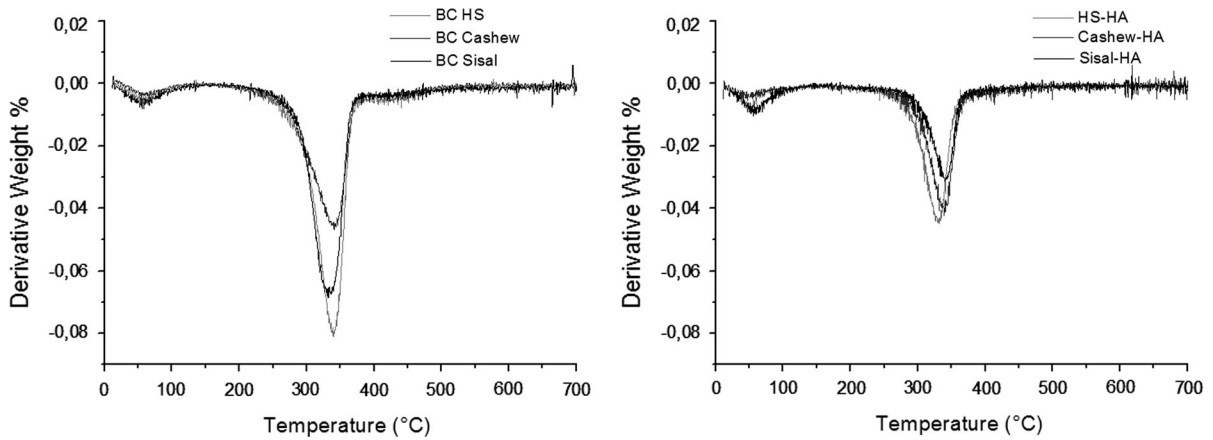


Fig. 1 dTG Curves of BC and BC–HA composites

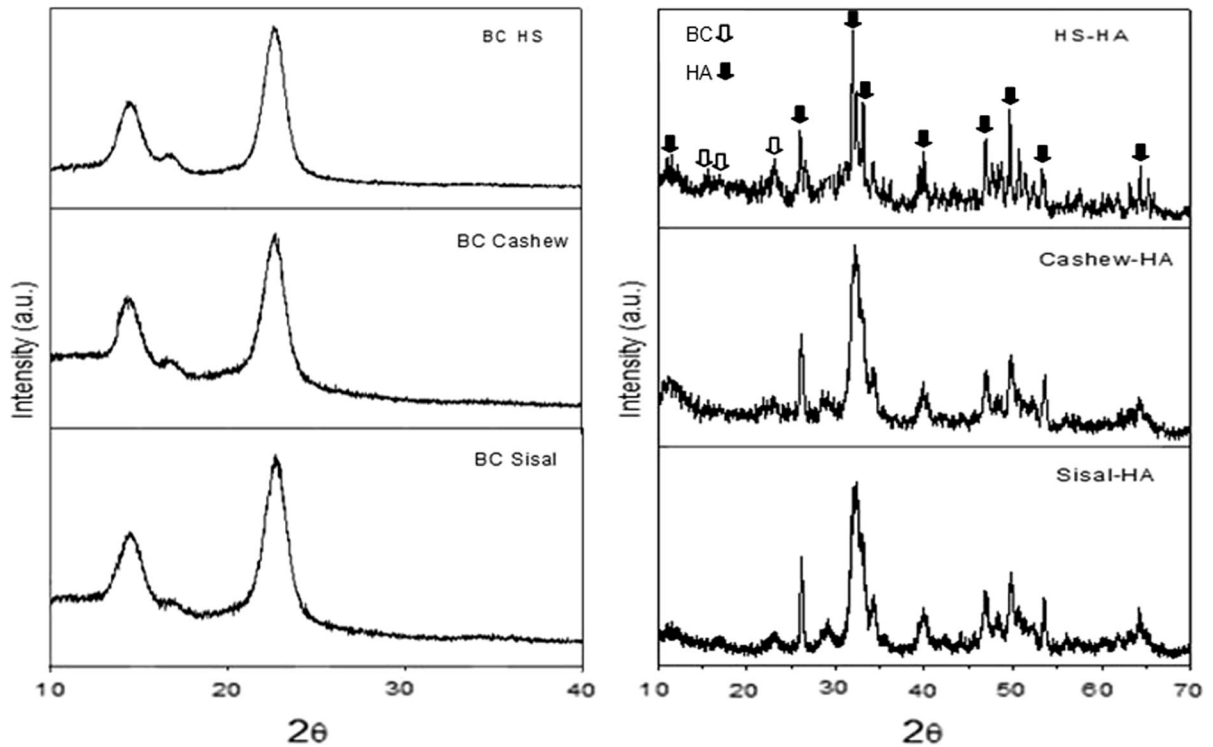


Fig. 2 X-ray diffraction patterns of BC and BC–HA composites

(Barud et al. 2008b), while the main characteristic diffraction peaks of HA were observed at $2\theta = 29^\circ, 32^\circ, 40^\circ,$ and 51° (Fig. 2). The crystallinity of HA in the composites was 38.3 % (HS-HA), 23.4 % (Cashew-HA), and 27.8 % (Sisal-HA). The poor crystalline apatite formation by biomimetic route is in agreement with literature (Roveri et al. 2010).

Fourier transform infrared spectroscopy (FTIR) studies

Expected cellulose vibrational bands were found in the FTIR spectra (Fig. 3; Table 3) of the BC pellicles and BC–HA composites. The pellicle purification was effective, since no additional bands, which could be related to contaminant substances, were detected.

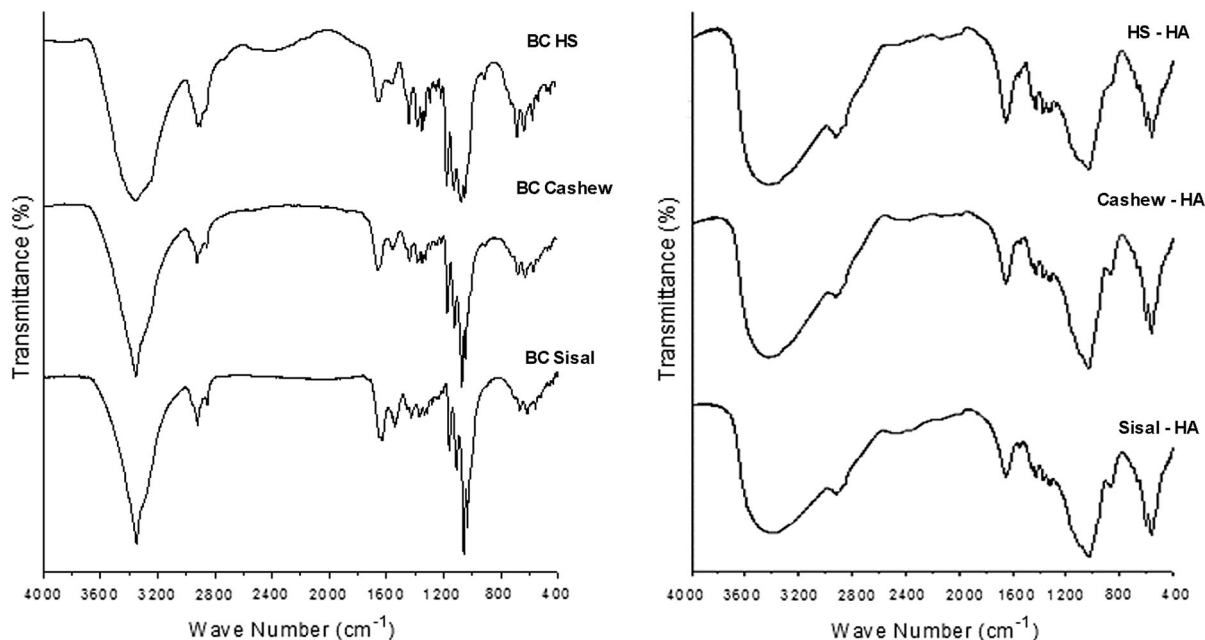


Fig. 3 FTIR spectrum of BC and BC–HA composites

The band in the region $3500\text{--}3200\text{ cm}^{-1}$, assigned to cellulose hydroxyl groups, was observed to have decreasing relative intensity and band broadening for the composite in comparison with the pure BC membrane. This evidence suggests that the presence of HA crystals affects the cellulose hydroxyl groups. Moreover, deviation of the band assigned to intramolecular hydrogen bonding ($\sim 3500\text{ cm}^{-1}$) confirms the strong interaction between the OH groups and apatite. It is important to emphasize that the presence of remanent water molecules may also have some influence on broadening of OH region.

The characteristic bands of phosphate group (PO_4^{3-}) at $569\text{--}573$, $601\text{--}603$, and 1030 cm^{-1} (Table 3) indicate the formation of HA (Zhai et al. 2005; Barrère et al. 2006). The presence of the PO_4^{3-} doublet band at 602 and 561 cm^{-1} suggests that the precursor phase of the HA was octacalcium phosphate (OCP), $\text{Ca}_8\text{H}_2(\text{PO}_4)_6 \cdot 5\text{H}_2\text{O}$ (Saska et al. 2011). OCP has a chemical structure close to HA, $\text{Ca}_{10}(\text{PO}_4)_6(\text{OH})_2$ and is considered a biological precursor of HA. Several studies have been performed to understand the role played by OCP in the formation of the mineral phase of calcified tissues and in the processes of bone

Table 3 Assignments of FTIR spectra of BC and BC–HA composites

BC–band assignments	Wavenumber (cm^{-1})		
	HS	Cashew	Sisal
ν (O–H), Cellulose I α	3350	3348	3346
ν (CH); ν_a (CH ₂)	2897	2918	2920
C (O–H), water absorption	1637	1647	1628
δ (HCH,OCH), in the plane	1429	1427	1425
CH, angle deformation	1371	1371	1371
C–O–H	1337	1337	1337
ν (CH ₂), in the plane	1317	1315	1315
ν_a (C–O–C), CH deformation	1163	1163	1161
ν (C–C), polysaccharides cellulose	1111	1111	1111
δ (C–O) in C–O–H, carbohydrate	1061	1061	1059
δ (C–O–H), outside the plane	669	665	669
BC–HA–band assignments	Wavenumber (cm^{-1})		
	HS-HA	Cashew-HA	Sisal-HA
ν (O–H)	3429	3423	3411
ν_3 (P–O)	1034	1032	1032
ν (CO_3^{2-})	874	872	872
ν_4 (O–P–O)	561; 602	561; 602	561; 602
ν stretching, ν_a asymmetric stretching, δ bond			

remodeling (Suzuki 2010; Elliot 1994). Moreover, the band, which was $\sim 877\text{ cm}^{-1}$, corresponds to the stretching mode of CO_3^{2-} ions, suggesting absorption of CO_2 from the air (Saska et al. 2011). Thus, the FTIR peaks at around $872\text{--}874\text{ cm}^{-1}$ indicate carbonated apatite deposition on BC substrates.

Generally, there were no differences among the BC spectra and among the BC–HA composite spectra. This observation confirms the similarities between the BC from different media and the similarities between the HA deposition on all BC nanofibers.

SEM and EDS

A typical dry BC membrane is depicted in Fig. 4a with a continuous network containing ultra-thin fibers (nanocellulose). The mean fiber diameter in BC pellicles was measured as about $92.2 \pm 4.2\text{ nm}$ (HS), $92.3 \pm 4.7\text{ nm}$ (Sisal) and $84.5 \pm 3.6\text{ nm}$ (Cashew) as measured using ImageJ. The SEM images

confirmed the characteristic three-dimensional BC structure, as well as the absence of contaminants. Moreover, there were no significant differences between the membranes from different media.

This nanostructure provides a large surface area for stabilization of adsorbed particles on it (Saska et al. 2011). The SEM images of the dry membranes of BC–HA nanocomposites (Fig. 4b–d) depict typical clustered crystallites, as described by others authors (Morejón-Alonso et al. 2007, 2008), precipitated on the BC. Although the HA crystal exhibited a larger particle size distribution (Fig. 4c), most of them were in the microscale ($\sim 2\text{ }\mu\text{m}$).

From all the EDS analysis of the BC pellicles (Table 4), the major components were carbon ($\sim 53\%$ w/wt) and oxygen ($\sim 44\%$) with some minor content of adsorbed ions from the culture media and washing solutions. The BC–HA nanocomposites presented a Ca/P mass ratio ranging from 1.53 to 1.58. The ratio of Ca/P is one of the methods used to

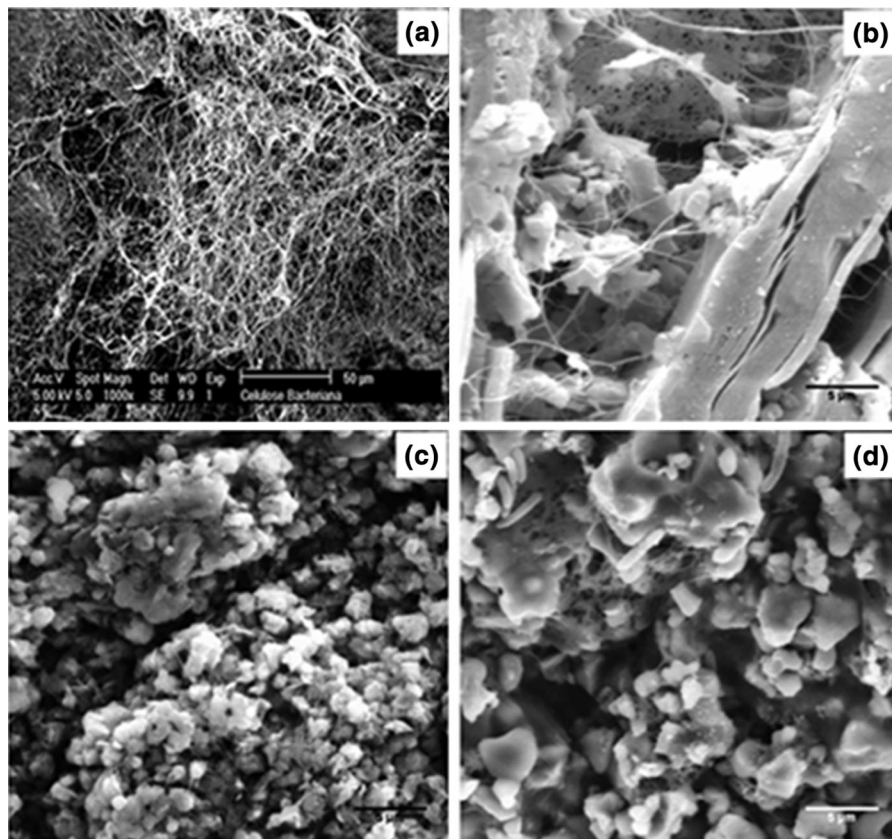


Fig. 4 Micrograph of dried **a** bacterial cellulose sheet and BC–HA composites **b** HS–HA, **c** Cashew–HA, **d** Sisal–HA

Table 4 EDS analysis of bacterial cellulose obtained from HS medium, cashew juice and sisal juice, and their hydroxyapatite composites

Element	Bacterial cellulose (mass%)		
	HS	Cashew	Sisal
C	53.02 ± 0.16	53.25 ± 0.00	53.24 ± 0.16
O	44.21 ± 0.39	43.67 ± 0.17	43.91 ± 0.21
Na	1.14 ± 0.15	1.35 ± 0.08	1.23 ± 0.06
P	–	–	–
Cl	1.15 ± 0.15	1.37 ± 0.01	1.38 ± 0.16
Ca	0.47 ± 0.07	0.38 ± 0.10	0.24 ± 0.17
Element	Composite bacterial cellulose-hydroxyapatite (mass%)		
	HS-HA	Cashew-HA	Sisal-HA
C	10.79 ± 0.71	9.36 ± 0.14	12.23 ± 0.72
O	41.55 ± 0.58	53.29 ± 0.37	45.92 ± 0.22
Na	1.35 ± 0.98	3.31 ± 0.11	3.53 ± 0.11
P	17.69 ± 0.26	12.56 ± 0.60	13.76 ± 0.20
Cl	1.20 ± 0.52	2.24 ± 0.32	2.87 ± 0.84
Ca	27.43 ± 0.41	19.24 ± 0.12	21.70 ± 0.29

Table 5 In vitro assays results of bacterial cellulose-hydroxyapatite (BC–HA) nanocomposites

	Desorption assay Mass (g)		
	HS-HA	Sisal-HA	Cashew-HA
Initial	0.0120 ± 0.0006	0.0084 ± 0.0002	0.0128 ± 0.0003
Final	0.0121 ± 0.0003	0.0083 ± 0.0002	0.0128 ± 0.0001
	Bioactivity assessment Mass (mg)		
	BC HS	BC Sisal	BC Cashew
Initial	4.8 ± 0.1	4.3 ± 0.1	3.9 ± 0.1
Final	8.6 ± 0.1	7.7 ± 0.3	6.8 ± 0.1
	HS-HA		
	HS-HA	Sisal-HA	Cashew-HA
Initial	51.8 ± 1.6	39.1 ± 6.2	37.7 ± 2.0
Final	61.0 ± 2.1	47.5 ± 5.4	46.4 ± 2.0
	Protein (BSA) adsorption Mass (mg)		
	HS-HA	Sisal-HA	Cashew-HA
Initial	–	–	–
Final	47.7 ± 5.1	59.5 ± 3.8	43.4 ± 2.0

characterize the composition of the different calcium phosphates, especially apatite, which may vary in composition. The formula of stoichiometric HA is $\text{Ca}_{10}(\text{PO}_4)_6(\text{OH})_2$, with a Ca/P mass ratio around 1.67. The Hutchens technique (Hutchens et al. 2006) involves the production of non-stoichiometric HA, reflecting the mineral formation of a calcium-deficient specimen.

The EDS, XRD, and FTIR results indicate that the deposited material is calcium-deficient carbonate-containing hydroxyapatite (CDHA), which is a similar phase to the biological apatite. This phase is desirable to facilitate the proliferation of osteoblast cells, which will synthesize the organic component for bone matrix regeneration (Le Guéhennec et al. 2004).

Desorption study

After 30 days of saline solution immersion, all the BC–HA nanocomposites presented no statistical difference (p value > 0.05) between the initial and the final mass (Table 5). Thus, there is no sign of HA

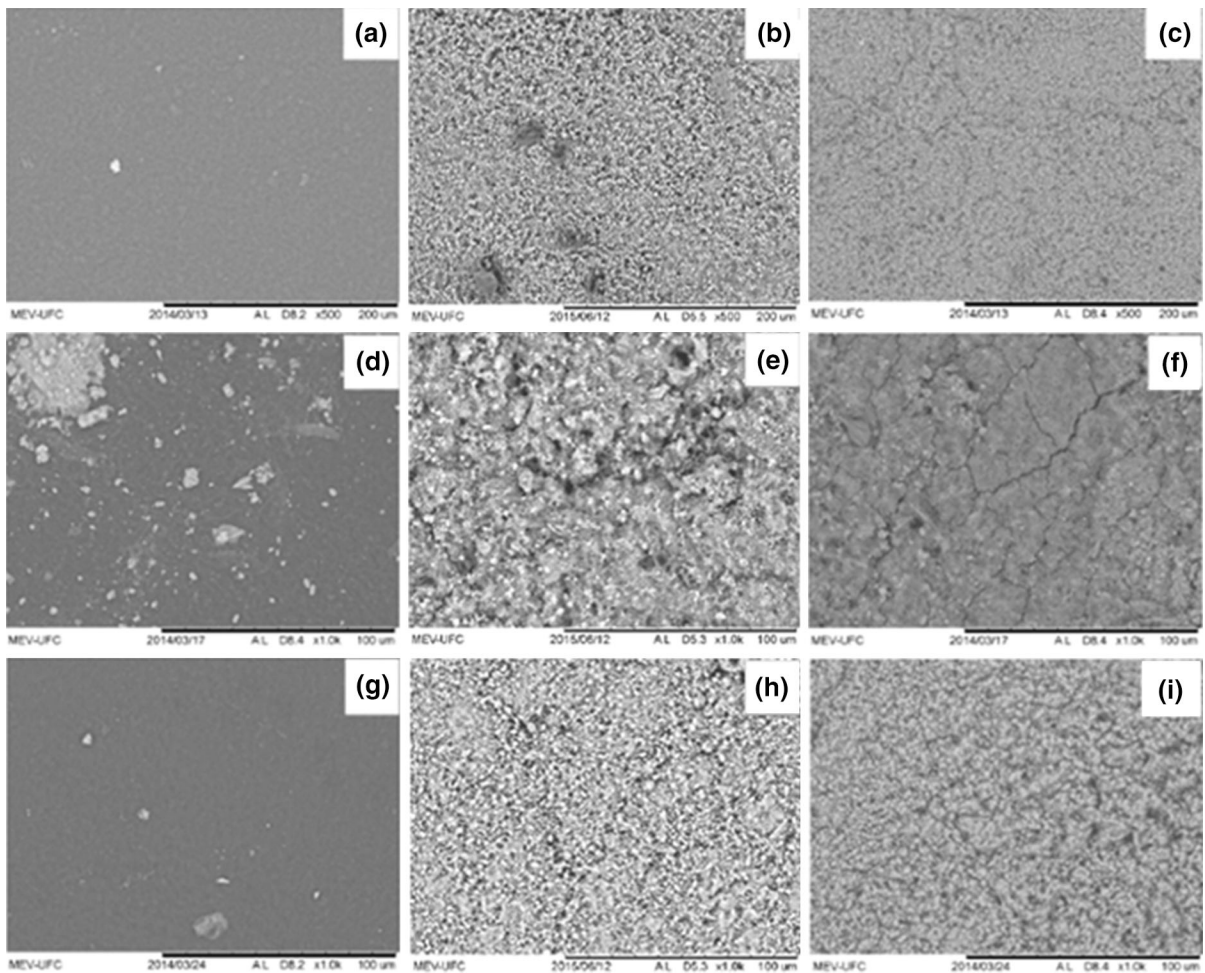


Fig. 5 Micrographs of BC films **a, d, g**, BC–HA composites **b, e, h** before immersion in SBF, and BC–HA composites **c, f, i** after immersion in SBF during 14 days. **a–c** HS; **d–f** Cashew; **g–i** Sisal

desorption from the composite. Loose particles can lead to particle migration which may result in damage to surrounding tissues (Mohamed 2012).

Kim et al. (2004) observed a weight loss of up to 25 % after 160 h of in vitro degradation of a HA/poly(ϵ -caprolactone) composite (Kim et al. 2004), while Alge et al. (2012) noted that the dicalcium phosphate dihydrate cement had a mass loss between 5 and 20 % in 2 weeks. These findings provide evidence that BC could hold the HA crystals in a way that prevented leaching (Alge et al. 2012).

Bioactivity assessment

The formation of a HA layer on the surface of composite materials after immersion in SBF (Fig. 5;

Table 5) attests the composite bioactivity. BC films are smooth (Fig. 5a, d, and g), in contrast to BC–HA composites (Fig. 5b, e, and h), which have a rough and granular surface. After immersion in the SBF (Fig. 5c, f, and i), the composites appear to be less granular and more smooth, because of the formation of the HA layer, increasing the crystal size and cementing the voids between the granules. Materials that exhibit this property have potential for use in bone tissue regeneration (Coleman et al. 2007).

Hydroxyapatite crystals can act as nucleation points, helping ion precipitation and increasing the mass of the composite. The mass gain in the BC–HA (8.4–9.2 mg) was superior to the BC pellicles (2.9–3.8 mg). Moreover, the percent increment was superior in the BC pellicles made from sisal juice

(21.5 %) and cashew juice (23.1 %) than in the BC from HS medium (17.8 %). This corroborates the notion that *G. hansenii* produced similar materials in synthetic and natural media.

Protein (BSA) adsorption

BSA adsorption in the BC–HA nanocomposites (Table 5) indicates the biomaterial from sisal juice had a higher index of protein adsorption, followed by HS and cashew juice. When a foreign material comes into contact with the body, proteins will immediately adsorb on its surface, and the adsorbed protein layer will determine future events, such as platelet adhesion, aggregation, or inflammatory response (Wang et al. 2012). Basu et al. (2013) observed an adsorption of about 51.3 mg of BSA per scaffold gram (Basu et al. 2013), similar to the data from this article, and Swain and Sarkar (2013) verified an adsorption between 23 and 28 % mg/g in different kinds of HA crystals (Swain and Sarkar 2013).

The tissue response to implanted materials arises mainly from differences in the adsorption of proteins that, in turn, depend on parameters of the surface topography, such as roughness, porosity, and pore size, as well as chemical composition among other factors. The BSA deposition in the BC–HA is due to the electrostatic interaction between the Ca^{2+} and the PO_4^{3-} of HA with the COO^- and the NH_3^+ of the BSA protein, respectively. All the nanocomposites presented good protein deposition properties, indicating possible osteoinductivity capacity.

Conclusion

Bacterial celluloses from agro-waste juices were similar to each other and to the standard culture medium. The HA nanocomposites with celluloses also did not exhibit substantial variation. HA was deposited with some uniformity in the spaces between the fibers of biopolymers and exhibited similar chemical characteristics to biological apatite. Preliminary in vitro studies showed that materials were biocompatible. In general, the BC membranes proved to be suitable for the preparation of nanocomposites for applications in the biomedical field.

Acknowledgments The authors are thankful to the Brazilian Research Agency EMBRAPA and the following laboratories

from Federal University of Ceará (UFC): Laboratory of Biomaterials, Laboratory of Characterization of Materials (LACAM), X-rays Laboratory, and Laboratory of Bioinorganic. This research was financially supported by the following fellowships: Fundação Cearense de Apoio ao Desenvolvimento Científico e Tecnológico (FUNCAP, Brazil), and Coordenação de Aperfeiçoamento de Pessoal de Nível Superior (CAPES, Brazil).

References

- Alge DL, Goebel WS, Chu TMG (2012) In vitro degradation and cytocompatibility of dicalcium phosphate dihydrate cements prepared using the monocalcium phosphate monohydrate/hydroxyapatite system reveals rapid conversion to HA as a key mechanism. *J Biomed Mater Res B Appl Biomater* 100B:595–602
- Andrade FK, Pértile RAN, Dourado F, Gama FMP (2010) Bacterial cellulose: properties, production and applications. In: Lejeune A, Deprez T (eds) *Cellulose: structure and properties, derivatives and industrial uses*. Nova Science Publishers, Hauppauge, pp 427–458
- Andrade FK, Alexandre N, Amorim I, Gartner F, Maurício AC, Luís AL et al (2012) Studies on the biocompatibility of bacterial cellulose. *J Bioact Compat Polym* 28:97–112
- Barrère F, Blitterswijk CA, Groot K (2006) Bone regeneration: molecular and cellular interactions with calcium phosphate ceramics. *Int J Nanomed* 1:317–332
- Barud HS, Ribeiro C, Crespi M, Martines M, Dexpert-Ghys J, Marques R et al (2007) Thermal characterization of bacterial cellulose-phosphate composites membranes. *J Therm Anal Calorim* 87:815–818
- Barud HS, Assunção RMN, Martines MAU, Dexpert-Ghys J, Marques RFC, Messaddeq Y et al (2008a) Bacterial cellulose-silica organic-inorganic hybrids. *J Sol Gel Sci Technol* 46:363–367
- Barud HS, de Araújo Júnior AM, Santos DB, de Assunção RMN, Meireles CS, Cerqueira DA et al (2008b) Thermal behavior of cellulose acetate produced from homogeneous acetylation of bacterial cellulose. *Thermochim Acta* 471:61–69
- Basu B, Swain SK, Sarkar D (2013) Cryogenically cured hydroxyapatite-gelatin nanobiocomposite for bovine serum albumin protein adsorption and release. *RSC Adv* 3:14622–14633
- Bohner M, Lemaître J (2009) Can bioactivity be tested in vitro with SBF solution? *Biomaterials* 30:2175–2179
- Bundela H, Bharadwaj V (2012) Synthesis and characterization of hydroxyapatite poly (vinyl alcohol) based nanocomposites for their perspective use as bone substitutes. *Polym Sci Ser A* 54:299–309
- Cavka A, Guo X, Shui-Jia T, Winstrand S, Jönsson LJ, Hong F (2013) Production of bacterial cellulose and enzyme from waste fiber sludge. *Biotechnol Biofuels* 6:1–10
- Chawla PR, Bajaj IB, Survase SA, Singhal RS (2009) Microbial cellulose: fermentative production and applications. *Food Technol Biotechnol* 47:107–124
- Coleman NJ, Nicholson JW, Awosanya K (2007) A preliminary investigation of the in vitro bioactivity of white Portland cement. *Cement Concrete Res* 37:1518–1523

- Elliot JC (1994) Structure and chemistry of the apatite and other calcium orthophosphates, 1st edn. Elsevier, Amsterdam
- Fang B, Wan YZ, Tang TT, Gao C, Dai KR (2009) Proliferation and osteoblastic differentiation of human bone marrow stromal cells on hydroxyapatite/bacterial cellulose nanocomposite scaffolds. *Tissue Eng Part A* 15:1091–1098
- Fricain JC, Granja PL, Barbosa MA, de Jeso B, Barthe N, Baquey C (2002) Cellulose phosphates as biomaterials. In vivo biocompatibility studies. *Biomaterials* 23:971–980
- Giannoudis PV, Dinopoulos H, Tsiridis E (2005) Bone substitutes: an update. *Injury* 36:S20–S27
- Gomes FP, Silva NHCS, Trovatti E, Serafim LS, Duarte MF, Silvestre AJD et al (2013) Production of bacterial cellulose by *Glucanacetobacter sacchari* using dry olive mill residue. *Biomass Bioenerg* 55:205–211
- Grande CJ, Torres FG, Gomez CM, Carmen Baño MC (2009) Nanocomposites of bacterial cellulose/hydroxyapatite for biomedical applications. *Acta Biomater* 5:1605–1615
- He M, Chang C, Peng N, Zhang L (2012) Structure and properties of hydroxyapatite/cellulose nanocomposite films. *Carbohydr Polym* 87:2512–2518
- Helenius G, Backdahl H, Bodin A, Nannmark U, Gatenholm P, Risberg B (2006) In vivo biocompatibility of bacterial cellulose. *J Biomed Mater Res A* 76A:431–438
- Hestrin S, Schramm M (1954) Synthesis of cellulose by acetobacter-xylinum. 2. Preparation of freeze-dried cells capable of polymerizing glucose to cellulose. *Biochem J* 58:345–352
- Huang Y, Zhu C, Yang J, Nie Y, Chen C, Sun D (2014) Recent advances in bacterial cellulose. *Cellulose* 21:1–30
- Hutchens SA, Benson RS, Evans BR, O'Neill HM, Rawn CJ (2006) Biomimetic synthesis of calcium-deficient hydroxyapatite in a natural hydrogel. *Biomaterials* 27:4661–4670
- Janicki P, Schmidmaier G (2011) What should be the characteristics of the ideal bone graft substitute? Combining scaffolds with growth factors and/or stem cells. *Injury* 42:S77–S81
- Kim HW, Knowles JC, Kim HE (2004) Hydroxyapatite/poly(ϵ -caprolactone) composite coatings on hydroxyapatite porous bone scaffold for drug delivery. *Biomaterials* 25:1279–1287
- Landi E, Tampieri A, Celotti G, Sprio S (2000) Densification behaviour and mechanisms of synthetic hydroxyapatites. *J Eur Ceram Soc* 20:2377–2387
- Le Guéhennec L, Layrolle P, Daculsi G (2004) A review of bioceramics and fibrin sealant. *Eur Cell Mater* 8:1–10
- Mohamed KR (2012). Biocomposite materials, composites and their applications. In: Prof. Ning H (ed.) *InTech*, pp 113–146
- Moore WR, Graves SE, Bain GI (2001) Synthetic bone graft substitutes. *ANZ J Surg* 71:354–361
- Morejón-Alonso L, Carrodegua RG, García-Menocal JAD, Pérez JAA, Manent SM (2007) Effect of sterilization on the properties of CDHA-OCP- β -TCP biomaterial. *Mater Res* 10:15–20
- Morejón-Alonso L, Carrodegua RG, García-Menocal JAD (2008) Transformations in CDHA/OCP/ β -TCP scaffold during ageing in simulated body fluid at 36.5 °C. *J Biomed Mater Res B Appl Biomater* 84B:386–393
- Nge TT, Sugiyama J, Bulone V (2010) Bacterial cellulose-based biomimetic composites. In: Elnashar M (ed) *Biopolymers*. InTech, Rijeka, pp 345–368
- Pértile RA, Moreira S, Costa RM, Correia A, Guardao L, Gartner F et al (2012) Bacterial cellulose: long-term biocompatibility studies. *J Biomater Sci Polym* 23:1339–1354
- Rivas B, Moldes AB, Dominguez JM, Parajo JC (2004) Development of culture media containing spent yeast cells of *Debaryomyces hansenii* and corn steep liquor for lactic acid production with *Lactobacillus rhamnosus*. *Int J Food Microbiol* 97:93–98
- Roveri N, Foresti E, Lelli M, Lesci IG, Marchetti M (2010) Microscopic investigations of synthetic biomimetic hydroxyapatite. *Microsc Sci Technol Appl Educ* 3:1868–1879
- Saska S, Barud HS, Gaspar AMM, Marchetto R, Ribeiro SJL, Messaddeq Y (2011) Bacterial cellulose-hydroxyapatite nanocomposites for bone regeneration. *Int J Biomater* 2011:1–8
- Schumann DA, Wippermann J, Klemm DO, Kramer F, Koth D, Kosmehl H et al (2009) Artificial vascular implants from bacterial cellulose: preliminary results of small arterial substitutes. *Cellulose* 16:877–885
- Segal L, Creely JJ, Martin AE, Conrad CM (1959) An empirical method for estimating the degree of crystallinity of native cellulose using the X-ray diffractometer. *Text Res J* 29:786–794
- Suzuki O (2010) Octacalcium phosphate: osteoconductivity and crystal chemistry. *Acta Biomater* 6:3379–3387
- Swain SK, Sarkar D (2013) Study of BSA protein adsorption/release on hydroxyapatite nanoparticles. *Appl Surf Sci* 286:99–103
- Uesu NY, Pineda EA, Hechenleitner AA (2000) Microcrystalline cellulose from soybean husk: effects of solvent treatments on its properties as acetylsalicylic acid carrier. *Int J Pharm* 206:85–96
- Wan YZ, Huang Y, Yuan CD, Raman S, Zhu Y, Jiang HJ et al (2007) Biomimetic synthesis of hydroxyapatite/bacterial cellulose nanocomposites for biomedical applications. *Mat Sci Eng C Bio S* 27:855–864
- Wang K, Zhou C, Hong Y, Zhang X (2012) A review of protein adsorption on bioceramics. *Interface Focus* 2:259–277
- Wippermann J, Schumann D, Klemm D, Kosmehl H, Salehi-Gelani S, Wahlers T (2009) Preliminary results of small arterial substitute performed with a new cylindrical biomaterial composed of bacterial cellulose. *Eur J Vasc Endovasc Surg* 37:592–598
- Wu JM, Liu RH (2013) Cost-effective production of bacterial cellulose in static cultures using distillery wastewater. *J Biosci Bioeng* 115:284–290
- Zadegan S, Hosainalipour M, Rezaie HR, Ghassai H, Shokrgozar MA (2011) Synthesis and biocompatibility evaluation of cellulose/hydroxyapatite nanocomposite scaffold in 1-n-allyl-3-methylimidazolium chloride. *Mater Sci Eng C* 31:954–961
- Zhai Y, Cui FZ, Wang Y (2005) Formation of nano-hydroxyapatite on recombinant human-like collagen fibrils. *Curr Appl Phys* 5:429–432
- Zimmermann KA, LeBlanc JM, Sheets KT, Fox RW, Gatenholm P (2011) Biomimetic design of a bacterial cellulose/hydroxyapatite nanocomposite for bone healing applications. *Mater Sci Eng C* 31:43–49